

Soft Matter

Accepted Manuscript



This is an *Accepted Manuscript*, which has been through the Royal Society of Chemistry peer review process and has been accepted for publication.

Accepted Manuscripts are published online shortly after acceptance, before technical editing, formatting and proof reading. Using this free service, authors can make their results available to the community, in citable form, before we publish the edited article. We will replace this *Accepted Manuscript* with the edited and formatted *Advance Article* as soon as it is available.

You can find more information about *Accepted Manuscripts* in the [Information for Authors](#).

Please note that technical editing may introduce minor changes to the text and/or graphics, which may alter content. The journal's standard [Terms & Conditions](#) and the [Ethical guidelines](#) still apply. In no event shall the Royal Society of Chemistry be held responsible for any errors or omissions in this *Accepted Manuscript* or any consequences arising from the use of any information it contains.

ARTICLE

Leidenfrost vapour layer moderation of drag crisis and trajectories of superhydrophobic and hydrophilic spheres falling in water.

Cite this: DOI: 10.1039/x0xx00000x

Received 00th January 2014,
Accepted 00th January 2014

DOI: 10.1039/x0xx00000x

www.rsc.org/

Ivan U. Vakarelski^a, Derek Y.C. Chan^{b,c} and Sigurdur T. Thoroddsen^a

We investigate the dynamic effects of a Leidenfrost vapour layer sustained on the surface of heated steel spheres during free fall in water. We find that a stable vapour layer sustained on textured superhydrophobic surface spheres falling through 95°C water can reduce the hydrodynamic drag by up to 75% and stabilize the sphere trajectory for Reynolds number between 10^4 - 10^6 , spanning the drag crisis in the absence of the vapour layer. For hydrophilic spheres under the same conditions, the transition to drag reduction and trajectory stability occurs abruptly at a temperature different from the static Leidenfrost point. The observed drag reduction effects are attributed to the disruption of the viscous boundary layer by the vapour layer whose thickness depends on the water temperature. Both the drag reduction and the trajectory stabilization effects are expected to have significant implications for development of the sustainable vapour layers based technologies.

1 Introduction

The traditional Leidenfrost effect^{1,2} refers to the long lifetime and high lateral mobility of small drops of liquid that are deposited on a very hot surface. The vapour layer that levitates the drop provides thermal insulation and lubricity and is stable as long as the surface temperature, T_S is above the Leidenfrost temperature, T_L that is significantly higher than the boiling point of the liquid. Correspondingly, a hot body at a temperature above T_L that is fully immersed in liquid will be in the Leidenfrost state, being completely enveloped by a vapour layer that separates it from the liquid, as demonstrated in Fig. 1a for a stationary hot steel sphere in water. When the sphere cools to below T_L , the vapour layer collapses and the resulting solid-liquid contact is manifested as a spectacularly explosive Leidenfrost transition shown in Fig. 1b.³ Hydrodynamic drag reduction by such intact gas layer on textured superhydrophobic surface is a topic of intense current research interest.⁴⁻⁷ It is a dynamic analogue of the non-wetting Cassie-Baxter state of water on superhydrophobic surfaces^{8,9} that stimulated recent studies on the combined effects of surface wettability and the Leidenfrost phenomenon.^{3,10-13}

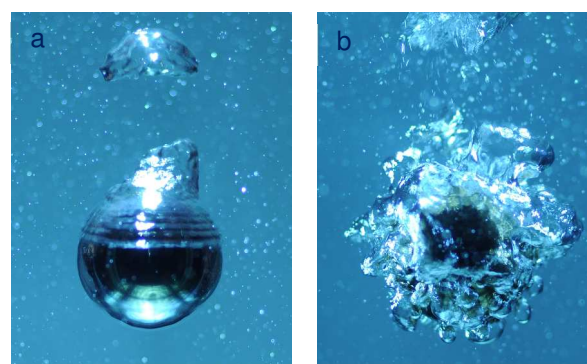


Figure 1. Snapshots of a stationary 20 mm hydrophilic steel sphere cooling in 95 °C water. (a) The sphere temperature, T_S is above the Leidenfrost temperature, $T_L = 260$ °C. The Leidenfrost state is characterized by a thin vapour layer streams around the sphere accompanied by vapour bubble pinch off at the upper apex. (b) The explosive Leidenfrost transition as the vapour layer collapses when T_S reaches T_L . Thereafter, the sphere cools rapidly to the pool temperature. (See also reference 3 that contains videos of the process).

It is well-known that surface modifications such as dimples on the surface of golf balls, the riblet structures on the skin of fast swimming sharks or the addition of small amounts of soluble

polymers in water can reduce the hydrodynamic drag on moving bodies.¹⁴⁻¹⁷ But despite potential benefits in energy efficient transport ranging from ocean liners to microfluidics, previous attempts to quantify drag reduction of spheres in water using surface gas layers produced only a moderate effect.¹⁸⁻²² Earlier, we have shown that a continuous Leidenfrost vapour layer on a heated steel sphere in a simple fluorocarbon liquid (FC-72 comprising mainly perfluorohexane C_6F_{14}) can reduce the hydrodynamic drag on falling sphere by up to 85%.²³ However, producing the same effect in water is far more challenging because it is very difficult to sustain a stable Leidenfrost vapour layer in water due to the higher vaporization heat capacity of water (30 times higher than FC-72) combined with higher boiling temperature (56°C for FC-72 vs 100°C for water) and higher surface tension (12 mN/m for FC-72 vs 72 mN/m for water). A further challenge highlighted in the present work is that the Leidenfrost temperature for a sphere falling through water is significantly higher than the static sphere Leidenfrost temperature.

In this paper we present results of a systematic investigation of the vapour layer induced drag reduction on spheres falling in water. Recent sphere cooling experiments in water³ and sessile drop experiments on a heated substrate¹⁰⁻¹² have demonstrated that the sustainability of the vapour layer depends strongly on the wetting properties of the solid surface. In fact, the cooling of an overheated superhydrophobic steel sphere in water can take place entirely in the continuous vapour layer or Leidenfrost regime, without transition to nucleated boiling and the accompanied vapour explosion that is always observed in the case of non-superhydrophobic surfaces.³ Therefore we seek to enhance the stability of the vapour layers by using textured superhydrophobic surfaces and conduct the experiments in water heated up to 95 °C as the thickness of such stable vapour layers also varies with the water temperature.

2 Experimental

In the present experiments we use high-speed video recording to measure the velocity of steel spheres with diameters, $d = 2R$ ranging from 10 mm to 40 mm falling through water held in a tank of height 2 m and cross-sectional dimensions 20 × 20 cm (Supplementary Fig. S1). Two types of sphere surfaces were used: smooth polished hydrophilic surface (water contact angle < 30°) and textured superhydrophobic surface (water contact angle > 160°).

2.1 STEEL SPHERES MODIFICATION.

The spheres used were polished stainless steel grinding balls (FRITSCH GmbH) of density $\rho_s = 7,700 \text{ kg m}^{-3}$ and diameters, $d = 10, 15, 20, 25, 30$ and 40 mm. The average surface roughness given by the manufacturer is $R_a < 0.06 \mu\text{m}$. Using an electrical discharge machine, we drilled a 0.5 mm diameter hole radially to the center of each sphere. A small metallic wire hook

was fitted in the hole to facilitate handling of the sphere without having to touch the sphere surface. The wire hook was also used to hang the sphere inside the heating furnace and to carry the heated sphere using metallic forceps. A thermal couple could also be inserted into the hole to measure the sphere temperature.

Spheres with a hydrophilic surface were prepared from the unmodified steel spheres after thorough washing with acetone, ethanol and water resulting in water contact angles of less than 10°. After heating of the sphere to temperature of about 500 °C the spheres remained hydrophilic with an average water contact angle of no more than 30°.

Spheres with superhydrophobic surfaces were made by application of a coating of a commercially available car mirror water-repellent agent (Glaco Mirror Coat “Zero”, Soft 99 Co.). The liquid coating is an alcohol-based suspension of silica nanoparticles functionalized by an organic hydrophobizing agent. A detailed description of the coating deposition procedure and characterization of the superhydrophobic coating properties is given in reference 3. In brief, the clean sphere was washed with the coating suspension liquid and then heat cured at about 300 °C for 30 minutes. Repeating the agent wash and heat cure process a further two times gave excellent superhydrophobic surface properties with a water contact angle of more than 160°. The coating has two scales of roughness: coarse scale with 0.5-2.0 μm structures of nanoparticle aggregates and a smaller nanoscale roughness that is characteristic of the size of the nanoparticles of about 50 nm.³

2.2 FREE FALLING SPHERES EXPERIMENTS.

The water tank and heater device used to conduct the falling sphere experiments was customer manufactured by ChangTong Science and Technology (TianJin) Co. LTD, China. A photograph of the device is given in Supplementary Fig. S1. The water tank is 2 m tall and has cross-sectional area 20 × 20 cm. The front and back walls of the tank are double-glazed fortified glass windows. The two side walls of the tank are also double-walled for improved thermal insulation. Electric heaters are installed in a heater chamber beneath the tank base that can heat the water in the tank up to boiling temperature of 100 °C. Thermocouple probes were used to monitor the water temperature inside the tank. After heating of the water to the desired temperature the electric heaters were switched-off during the falling sphere experiments to suppress water thermal convections and for safety considerations. Several minutes after the heaters were switched-off, the temperature of the water in the tank was found to be uniform to within $\pm 1 \text{ }^\circ\text{C}$ from the bottom to about 2 cm below the water surface at the top. The working temperature for the experiments was maintained to within $\pm 1 \text{ }^\circ\text{C}$ as measured at a control point about 20 cm below the water surface.

Spheres were heated to the desired temperature in a temperature control furnace for at least 30 minutes. The heated spheres were held by metal forceps and carefully released from below the water surface at the top of the tank. The sphere fall was monitored by a high-speed video camera (Photron Fastcam SA-3) with a typical filming frame rate of 1000 fps. The sphere trajectory coordinates vs time and the corresponding instantaneous velocity was determined by image processing the videos with the camera software (Photron FASTCAM Viewer, PFV Ver.3262). Example for the fall distance vs time data obtained by processing the sphere fall videos is given in Supplementary Fig. S3.

2.3 DETERMINATION OF THE DRAG COEFFICIENTS

The hydrodynamic drag on a sphere moving at velocity U is characterized in terms of the variation of standard drag coefficient defined by, $C_D = 2F_D/(\pi R^2 \rho U^2)$ with the Reynolds number, $Re = 2\rho R U/\mu$. Here F_D is the drag force on the sphere, ρ the fluid density, R the sphere radius and μ the dynamic shear viscosity of the fluid. In free falling sphere experiments, the drag coefficient is determined from the sphere terminal velocity, U_T using the relation:

$$C_D = (8[\rho_s - \rho]gR)/(3\rho U_T^2) \quad (1)$$

where g is the gravitational acceleration and ρ_s the sphere density. The terminal velocity was corrected for the effect of the tank walls using the following correction formula due to Newton (1687):

$$U_T/U_{T\infty} = [1 - (d/D)^2] [1 - 0.5(d/D)^2]^{1/2} \quad (2)$$

where U_T is the measured terminal velocity, $U_{T\infty}$ is the corrected terminal velocity for infinite flow domain, $d = 2R$ is the sphere diameter and D is the diameter of a cylindrical tank. For the $a \times a$ square cross-section tank used in the present experiment, the effective diameter D in eq. 2 is calculated by equating the areas of the circle and the square, i. e. $D = (2/\sqrt{\pi})a$.²⁴

2.4 SPHERE COOLING RATES

The temperature of the sphere that was held stationary under water was monitored by a thermocouple probe inserted into the sphere center. Further details for these measurements can be found in reference 3 that also contains supplementary videos of the cooling process in each case. The time dependence of the temperature of a 20 mm steel sphere cooling in 24 °C, 85 °C and in 95 °C water is shown in Fig. 2a for a hydrophilic sphere, and in Fig. 2b for a superhydrophobic sphere. For the hydrophilic sphere the results show an abrupt transition from Leidenfrost regime to nucleate boiling regime at the Leidenfrost temperature, T_L of about 440 °C in 24 °C water, T_L of about 280 °C in 85 °C water and at T_L of about 260 °C in 95 °C water

(Fig. S4a). This transition at the Leidenfrost point (LP in Fig 2a) is characterized by an explosive transition to the nucleated boiling regime (see Fig. 1b). As could be expected for the hydrophilic spheres the Leidenfrost temperature decreases with increasing pool temperature.²⁵ In the case of superhydrophobic sphere, the cooling is entirely in Leidenfrost regime without transition to nucleate boiling³ (Fig. 2b).

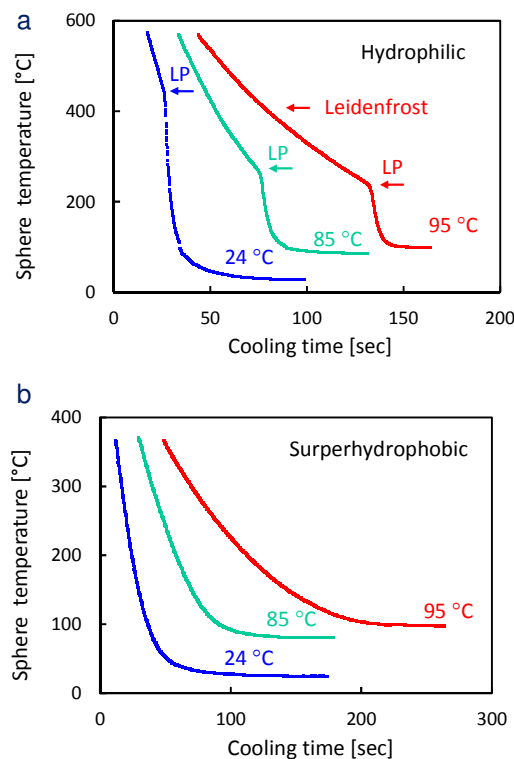


Figure 2. Sphere temperature vs cooling time for statically held 20 mm steel sphere cooling in 24 °C water (blue line), 85 °C (green line) or 95 °C water (red line): (a) hydrophilic sphere, (b) superhydrophobic sphere. Arrows on (a) mark the Leidenfrost point (LP) characterized by an explosive transition to the nucleated boiling regime.³ Supplementary Fig. S2 shows data for the corresponding heat transfer coefficients.

3 Results and discussions

3.1 TRIALS IN ROOM TEMPERATURE 95 °C AND 85 °C WATER.

In the initial trials we measured the velocity of heated steel spheres falling in water at 24 °C (room temperature). Fig. 3 shows data for the terminal velocity dependence on the spheres temperature in the case of 40 mm hydrophilic and superhydrophobic steel spheres ($Re \sim 1.0 \times 10^5 - 1.5 \times 10^5$). For the 40 mm hydrophilic sphere with initial sphere temperature between 300 °C and 700 °C we observed about a 35 % increase in the terminal velocity compared to the room temperature sphere (Fig. 3). However, the vapour layer around the falling hydrophilic sphere always collapsed shortly after sphere release even for spheres heated to 800 °C, well above the static sphere Leidenfrost temperature of about 440 °C (Fig. 2a). The collapse or destabilization of the Leidenfrost layer was confirmed visually as shortly after the sphere release, we observe a bubble cloud burst from the sphere surface. It can be assumed that the vapour layer destabilization is initiated by the shear stresses induced on the layer during the sphere fall. All the data points shown in Fig. 3 for the hydrophilic sphere should thus be regarded as results corresponding to an absence of a vapour layer. The drag reduction effect in that case is due to the combined effects of heating up of the water around the falling sphere resulting in a reduction of viscosity in the boundary layer and the shedding of small bubbles from the sphere surface that correspond to the regime of nucleate boiling. The relative contributions of these effects are not easy to quantify.

For 40 mm superhydrophobic spheres we measured a similar increase of about 35% in the terminal velocity with the increase of the sphere temperature to about 300 °C (Fig. 3). For the superhydrophobic sphere, the Leidenfrost vapour layer remained intact as we did not observe any destabilization or collapse of the vapour layer as the sphere fell. This in contrast to the case of the hydrophilic sphere, and one can assume that the drag reduction was due predominantly to the presence of the Leidenfrost regime vapour layer. However considering that the vapour free heated hydrophilic sphere shows a similar drag reduction it remains unclear if the drag reduction effect for the superhydrophobic sphere in 24 °C water is primary due to the vapour layer around the sphere or due to the heating of the water in the vicinity of the sphere.

In order to resolve the ambiguity in the interpretation of the data in room temperature water we chose to conduct experiments in water heated up to 95 °C water. In water heated near the boiling point, a stable vapour layer can be easily sustained on the falling sphere and at the same time the effect of the water heating by the spheres is negligible. An added advantage is that the viscosity of water at 95 °C is about three times lower than the water viscosity at room temperature and this helps to extend the experimental Reynolds numbers to beyond the critical value.

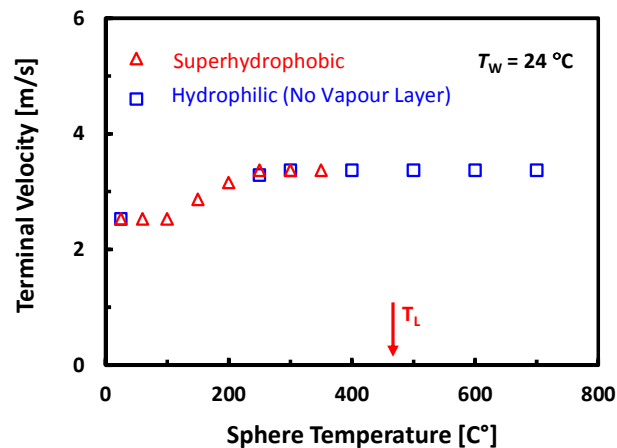


Figure 3. Variation of the terminal velocity with the sphere temperature measured for a 40 mm steel sphere falling through room temperature (24 °C) water. Open square data points (blue) are for hydrophilic sphere and open triangles data (red) are for superhydrophobic sphere. Notice that although a static hydrophilic sphere will be in Leidenfrost regime for $T_S > 440$ °C, the vapour layer is destroyed shortly after the sphere release to free fall even for spheres of initial T_S as high as 700 °C. All hydrophilic spheres data points thus represent the vapour layer free case.

In Fig. 4 we quantify the effects of surface treatment on the vapour layer by comparing the temperature variation of the terminal velocity of 20 mm diameter hydrophilic and superhydrophobic steel spheres falling in 95 °C water. For the hydrophilic sphere it was possible to sustain a stable vapour layer on the falling sphere for temperatures $T_S > 300$ °C that is only slightly higher than the static sphere Leidenfrost temperature of about 260 °C (Fig. 2b). This transition to the Leidenfrost regime is observed as a sharp increase of the terminal velocity of the sphere from about 1.9 m/s to about 3.8 m/s corresponding to a decrease of the drag force on the sphere by about 75 %. The dramatic speed difference is illustrated in the Supplementary Video 1. The drag reduction observed under this condition is of the same magnitude as that observed for Leidenfrost spheres falling in fluorinated liquid.²³ The results for the superhydrophobic sphere demonstrate that the additional textured superhydrophobic surface property enhances the Leidenfrost vapour layer stability under dynamic conditions so that drag reduction effect is observable even at a lower sphere temperature of 125 °C (25 °C overheat) and is fully developed above 150 °C (50 °C overheat).

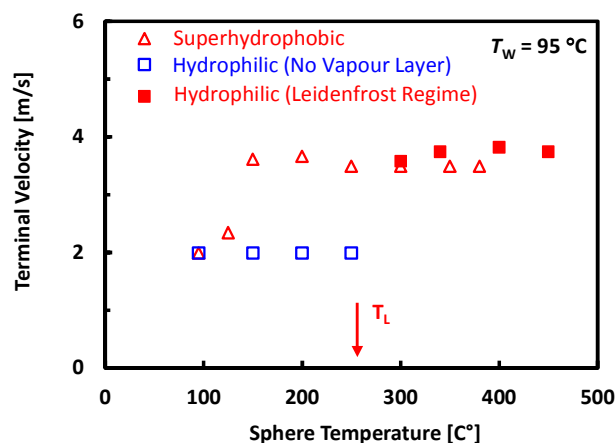


Figure 4. Variation of the terminal velocity with the sphere temperature, measured for a 20 mm steel sphere falling through 95 °C water. Open squares (blue) are data for hydrophilic spheres at temperature below the Leidenfrost temperature ($T_L = 260$ °C) and solid squares (red) for temperatures above T_L . Open triangles (red) are data for superhydrophobic spheres (see also Video 1).

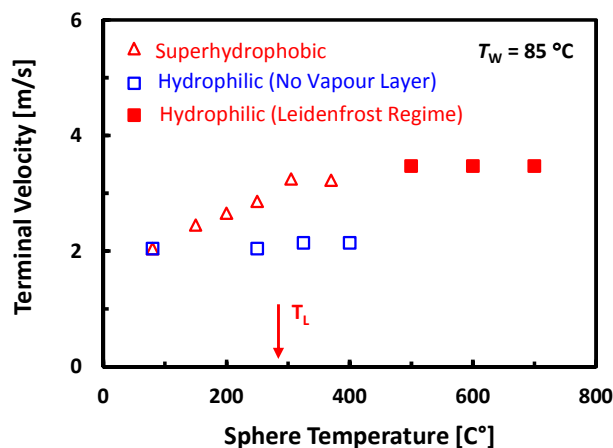


Figure 5. Variation of the terminal velocity with the sphere temperature, measured for a 20 mm steel sphere falling through 85 °C water. Data showing the gradual development of drag reduction for superhydrophobic spheres are shown in open (red) triangles. Data for hydrophilic spheres shows no drag reduction below 500 °C open (blue) squares and the sudden development of full drag reduction solid (red) squares above 500 °C for sphere falling in Leidenfrost regime. The static Leidenfrost temperature, $T_L \sim 280$ °C of the hydrophilic sphere in 85 °C water is indicated.

In Fig. 5, we present results for 20 mm spheres falling in water heated to about 85 °C which show transient behaviour between that for room temperature water and 95 °C water. In 85 °C water, the moving hydrophilic sphere does transition to a Leidenfrost regime but at temperature above 500 °C which is substantially higher than the static sphere Leidenfrost temperature, $T_L \sim 280$ °C (Fig. 2a). In contrast, drag reduction

for the superhydrophobic spheres is already noticeable at temperature of about 150 °C but becomes fully developed only at temperatures above 300 °C.

3.2 REYNOLDS NUMBER DEPENDENCE.

Next we elucidate the dependence of drag reduction on the Reynolds number by conducting experiment with different size steel spheres falling in 95 °C water. The experimental range of Reynolds numbers covered in these measurements: $10^4 < Re < 10^6$ (water at 95 °C, $\rho = 0.96$ kg m⁻³, $\mu = 0.03$ mPa s) spans the location of the drag crisis for a free falling solid sphere at which the drag coefficient C_D drops rapidly from 0.5 to 0.2 at $Re \sim 3 \times 10^5$.

In Fig. 6 we compare the drag coefficients for hydrophilic spheres at temperature $T_S = 95$ °C, the same temperature as the water where there is no vapour layer, with the drag coefficient of superhydrophobic spheres at $T_S = 200$ °C, at which a stable Leidenfrost vapour layer surrounds the sphere. The results for hydrophilic spheres (no vapour layer) follow closely literature data for solid spheres falling in water that exhibits the characteristic onset of the drag crises at the critical $Re \sim 3 \times 10^5$. This is associated with the rapid decrease of the drag coefficient from the sub-crisis value of about 0.5 through the minimum value of about 0.2.^{15,16} In contrast, superhydrophobic spheres in the Leidenfrost regime ($T_S = 200$ °C) with a surface vapour layer exhibit a gradual decrease in the drag coefficient for $Re > 10^4$ that follows the same trend demonstrated before for fluorinated liquid.²³

For spheres released from rest, the time dependence of the velocity, $U(t)$ is observed to evolve towards the terminal value, U_T according to the exponential form:¹⁶

$$U(t) = U_T(1 - e^{-t/\tau}) \quad (3)$$

As discussed in reference 16 this equation does not accurately present the complex dynamic of the true fall trajectory, but could be used as an effective tool to estimate the terminal velocity. Results for the drag coefficient shown in Fig. 6, shown as solid squares for no-vapour hydrophilic case and solid circles for Leidenfrost regime are calculated using the sphere velocity measured close to the bottom of the 2 m water tank. However, for higher Reynolds number ($Re > 2 \times 10^5$), the velocity after the 2 m fall has not yet reached the terminal value as detailed in Supplementary Fig. S4 data. In such cases, eq. (3) can be used to estimate the terminal velocity that is then used to calculate the corresponding drag coefficient and Reynolds number represented as open circles on Fig. 6. These extrapolated results indicate the gradually decreasing trend of the drag force with increasing Re in the Leidenfrost regime is valid up to the maximum investigated limit of $Re \sim 10^6$ exceeding the location of the drag crises minimum in the no vapour layer case.

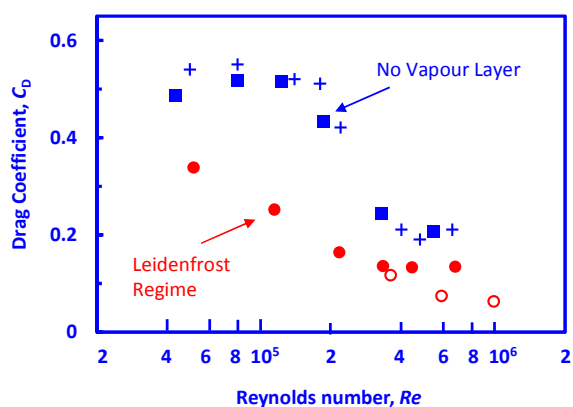


Figure 6. Dependence of the drag coefficient on the Reynolds number for steel spheres ($2R = 10; 15; 20; 25; 30; 40$ mm) falling in $95\text{ }^{\circ}\text{C}$ water. Solid squares (blue) are for hydrophilic spheres at a sphere temperature $T_s = 95\text{ }^{\circ}\text{C}$, hence no vapour layer is present, and solid circles (red) are for superhydrophobic spheres at a sphere temperature $T_s = 200\text{ }^{\circ}\text{C}$ in the Leidenfrost regime. Both sets of results are calculated using the sphere velocity at the end of the 2 m fall. Open circles (red) are for $200\text{ }^{\circ}\text{C}$ superhydrophobic spheres calculated using the extrapolated values for the terminal velocity (Supplementary Fig. S4). Literature values for smooth solid spheres falling in an “infinite” tank measured by White¹⁵ are shown as blue crosses.

3.3 STABILISATION OF THE FALL TRAJECTORY

We found that the Leidenfrost vapour layer not only reduces drag but also has a dramatic effect on the stability of the trajectory of the falling sphere. This is demonstrated in Fig. 7 for the case of 40 mm spheres falling in $95\text{ }^{\circ}\text{C}$ water. In the absence of the Leidenfrost vapour layer (Fig. 7a) the sphere trajectories exhibit large, random deviations from rectilinear motion that are due to non-axisymmetric, flow structures contained in the sphere wake^{26,27} that perturb the sphere trajectory. In contrast in the Leidenfrost regime the sphere fall trajectory is almost perfectly linear (Fig. 7b) and this is in accordance with smaller and more symmetrical wake observed behind spheres falling in Leidenfrost regime.²³ This is the first time we report this phenomenon that may prompt further investigations with important practical implication for the vapour layers drag reduction related applications. However, indications of this effect were evident in our earlier studies conducted in fluorinated liquids²³ even though they were not reported.

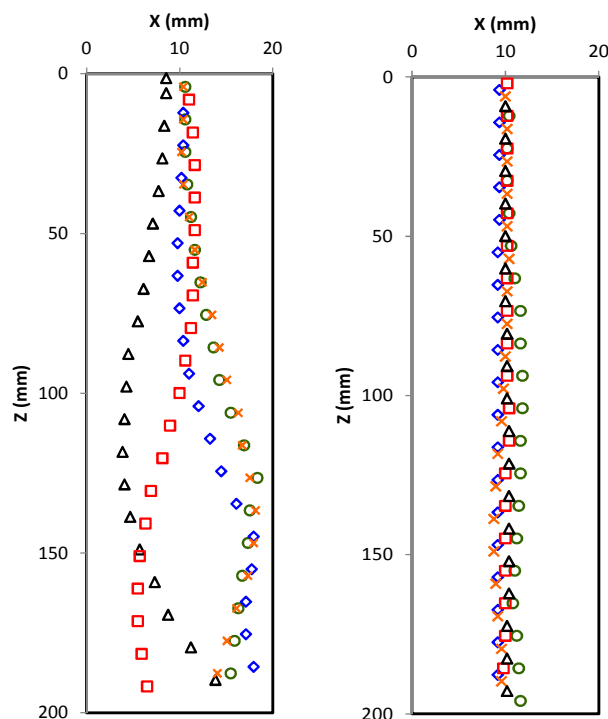


Figure 7. Examples of the trajectories of 40 mm steel falling spheres in $95\text{ }^{\circ}\text{C}$ water: (a) $T_s = 95\text{ }^{\circ}\text{C}$ hydrophilic spheres with no vapour layer, (b) $T_s = 200\text{ }^{\circ}\text{C}$ superhydrophobic spheres in the Leidenfrost regime in the presence of a vapour layer. The horizontal and vertical (X, Z) trajectory coordinates are obtained from high speed video recording of five independent runs with each trajectory represented by a different symbol.

3.4 CORRELATION WITH THE VAPOUR LAYER THICKNESS

For the range of the Reynolds number investigated here ($Re \sim 10^4 - 10^6$) the predominant component of the drag force on the sphere is due to the pressure-induced form or wake drag with the viscous or skin friction drag accounting for less than 5% of the total drag on the sphere.²⁸ In our earlier study,²³ we demonstrated the correlation between the reduction in the drag coefficient and the relocation of the separation point of the boundary layer towards the rear of the sphere in the Leidenfrost regime. It is well known that the drag crisis in the no-vapour layer case is associated with the moving of the flow separation point to the rear of the sphere when the transition to turbulent boundary layer occurs. Although the presence of the Leidenfrost vapour layer also moves the separation point, the underlying physical mechanism is due to changing the no-slip boundary condition for the solid-liquid boundary layer with one that might be closer to stress-free boundary condition for the vapour-liquid boundary layer.^{29,30}

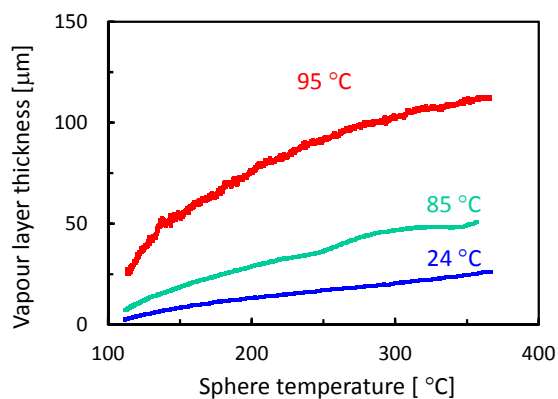


Figure 8. Vapour layer thickness vs sphere temperature for 20 mm superhydrophobic steel sphere cooling in 24 °C water (blue line), 85 °C (green line) and 95 °C water (red line), calculated using Fig. 2b data and eq. 4.

McHale et al.²² have reported correlations between the drag reduction on superhydrophobic surfaces of various texture and the thickness of the surface sustained air layer or plastron. However, in our experiment we found no change in the drag on unheated superhydrophobic sphere falling in room temperature water (Fig. 3). This indicates that the naturally sustained air layer on the type of superhydrophobic surface used here is not thick enough to provide measurable drag reduction effects. We can further quantify the vapour layer thickness effect by comparing the thickness of the Leidenfrost vapour layer to that of the viscous boundary layer. The thickness of the Leidenfrost vapour layer, δ_L can be estimated from the cooling rate in the Leidenfrost regime using the following relation:³¹

$$\delta_L = \left(\frac{3k_v}{\rho_s c_p R} \right) \frac{(T_s - T_{sat})}{(dT/dt)} \quad [4]$$

where $\rho_s = 7,700 \text{ kg m}^{-3}$ is the sphere density, $c_p = 466 \text{ J kg}^{-1} \text{ K}^{-1}$ is the sphere specific heat, (dT/dt) is the sphere cooling rate, $k_v = 0.016 \text{ W m}^{-1} \text{ s}^{-1}$ is the water vapour thermal conductivity and $T_{sat} = 100 \text{ °C}$ is the saturation temperature. Fig. 8 shows the vapour film thicknesses estimated using the static superhydrophobic spheres cooling rate data (Fig. 2b). As the sphere temperature T_s varies between 150 °C – 350 °C, we find $\delta_L \sim 50 \text{ } \mu\text{m} - 110 \text{ } \mu\text{m}$ in 95 °C water. The vapour layer thickness estimated from cooling rate data taken at 85 °C water is about 2.5 times thinner than that at 95 °C and this may account for the quantitative variation in drag reduction at different water temperatures. However, in both cases, the vapour layer thickness is comparable to the typical estimate for the viscous boundary layer thickness:²⁹

$$\delta_B \sim (2\mu R/\rho U_T)^{1/2} \sim 50 \text{ } \mu\text{m} \quad [5]$$

This would suggest that the Leidenfrost vapour layer acts as a surface feature with a variable characteristic length that is responsible for the gradual reduction in the drag coefficient

rather than an abrupt drag crisis transition for surface with fixed geometric features. A similar gradual reduction in the drag coefficient has also been reported when a low (5 ppm) concentration of polymer has been added to the water where polymer coil-stretching in the boundary layer is attributed as the drag reduction mechanism.¹⁶

Conclusions

This study has elucidated conditions under which large and sustained drag reduction and trajectory stabilization for hot steel spheres falling in water can be achieved using stable continuous vapour surface layers. Due to the high heat transfer coefficient of water compared to simple liquids, it is known to be difficult to sustain a stable vapour layer on moving surfaces. For hot spheres with a superhydrophobic surface, a stable vapour layer can always be maintained at the surface and full drag reduction is attained at a sphere temperature of $\sim 150 \text{ °C}$ in 95 °C water and $\sim 300 \text{ °C}$ in 85 °C water. We attribute this dependence on water temperature to the variations of the thickness of the stable vapour layer. The threshold thickness of the vapour layer for the development of the drag reduction is correlated with the thickness of the viscous boundary layer. For hot spheres with a hydrophilic surface, the transition to full drag reduction is sudden and occurs close to the static Leidenfrost temperature of $T_L \sim 260 \text{ °C}$ in 95 °C water. However, in 85 °C water, the transition occur at $\sim 500 \text{ °C}$, well above the static Leidenfrost temperature of $T_L \sim 280 \text{ °C}$. Thus the critical transition temperature to drag reduction for hydrophilic sphere differs from the familiar static Leidenfrost temperature. Finally, the drag reduction and the associated stabilization of fall trajectory operate at Reynolds numbers exceeding the drag crisis minimum observed in the absence of vapour layers. These results will hopefully help stimulate current effort to develop inexpensive drag reduction technologies based on the sustainability of air layer on textured superhydrophobic surface.

Acknowledgements

We acknowledge G. D. Li from KAUST Solar and Photovoltaics Research Center for assisting in the water tank and heater device design, and KAUST Machine Workshop for the support in setting the experiments. This work is support in part by an Australian Research Council Discovery Project Grant to DYCC.

Notes and references

^a Division of Physical Sciences and Engineering and Clean Combustion Research Centre, King Abdullah University of Science and Technology (KAUST), Thuwal 23955-6900, Saudi Arabia. E-mail: ivanuriev.vakarelski@kaust.edu.sa

^b Department of Mathematics and Statistics, The University of Melbourne, Parkville 3010, Australia.

^c Department of Chemistry and Biotechnology, Swinburne University of Technology, Hawthorn 3122, Australia.

Electronic Supplementary Information (ESI) available:

Supplementary pdf file containing Figs. S1-S4: Fig. S1. Photograph of the water vessel and heater device; Fig. S2 Heat transfer coefficients vs. sphere temperature dependences; Fig. S3. Examples for the fall distance vs time data; Fig. S4. Collection of velocity vs time data for 15 mm (a); 20 mm (b); 30 mm (c); 40 mm (e) spheres.

Video 1. This combined video parallels the fall of 20 cm steel sphere in 95 °C water: the left side is for 95 °C hydrophilic sphere and the right side is for 200 °C superhydrophobic sphere. Video is shot at the lower part of the tank where the spheres approach terminal velocity. The frame rate used was 1000 fps and the video playback speed is 30 fps.

1. J. G. Leidenfrost, *De Aquae Communis Nonnullis Qualitatibus Tractatus* (1756); J. G. Leidenfrost, *Intl. J. Heat Mass Transfer*, 1966, **9**, 1153.
2. D. Quéré, *Annu. Rev. Fluid Mech.* 2013, **45**, 197.
3. I. U. Vakarelski, N. A. Patankar, J. O. Marston, D. Y. C. Chan and S. T. Thoroddsen, *Nature*, 2012, **489**, 274.
4. J. P. Rothstein, *Annu. Rev. Fluid Mech.* 2010, **42**, 89.
5. G. McHale, M. I. Newton and N. J. Shirtcliffe, *Soft Matter*, 2010, **6**, 714.
6. H. Dong, M. Cheng, Y. Zhang, H. Wei and F. Shi, *J. Mater. Chem. A*, 2013, **1**, 5886.
7. B. Wang, J. Wang, Z. Dou and D. Chen, *Ocean Engineering*, 2014, **79**, 58.
8. A. B. D. Cassie and S. Baxter, *Trans. Faraday Soc.*, 1944, **40**, 0546.
9. D. Quere, *Annu. Rev. Mater. Res.*, 2008, **38**, 71.
10. G. Liu, L. Fu, A. V. Rode and V. S. J. Craig, *Langmuir*, 2011, **27**, 2595.
11. H. Kim, B. Truong, J. Buongiorno and L. Hu, *App. Phys. Letts.*, 2011, **98**, 083121 .
12. D. A. del Cerro, A. G. Marín, G. R. B. E. Romer, B. Pathiraj, D. Lohse, and Albertus J. H. Veld, *Langmuir*, 2012, **28**, 15106.
13. I. U. Vakarelski, D. Y. C. Chan, J. O. Marston and S. T. Thoroddsen, *Langmuir*, 2013, **29**, 11074.
14. P. W. Bearman and J. K. Harvey, *Aeronautical Q.*, 1976, **27**, 112.
15. A. White, *Nature*, 1965, **216**, 994.
16. N. Lyotard, W. L. Shew, L. Bocquet and J.-F. Pinton, *Eur. Phys. J. B*, 2007, **60**, 469.
17. B. Dean and B. Bhushan, *Phil. Trans. R. Soc. A*, 2010, **368**, 4775.
18. W. S. Bradfield, R. O. Barkdoll and J. T. Byrne, *Int. J. Heat. Mass Transfer.*, 1962, **5**, 615.
19. Y. Zvirin, G. R. Hewitt and D. B. R. Kenning, *Exp. Heat Transfer*, 1990, **3**, 185.
20. F. S. Gunnerson and P. R. Chappidi, in *Dynamic Aspects of Explosion Phenomena*, AIAA, New York, 1993, pp. 322-333.
21. L. Meyer, *Nucl. Eng. Des.*, 1999, **189**, 191.
22. G. McHale, N. J. Shirtcliffe, C. R. Evans and M. I. Newton *Appl. Phys. Lett.*, 2009, **94**, 064104.
23. I. U. Vakarelski, J. O. Marston, D. Y. C. Chan and S. T. Thoroddsen, *Phys. Rev. Lett.*, 2011, **106**, 214501.
24. R. P. Chhabra, P. H. T. Uhlherr and J. F. Richardson, *Chem. Eng. Sci.* 1996, **51**, 4531.
25. V. K. Dhir and G. P. Purohit, *Nucl. Eng. Des.* 1978, **47**, 49.
26. S. Taneda, *J. Fluid Mech.*, 1978, **85**, 187.
27. M. Horowitz and C. H. K. Williamson, *J. Fluid Mech.*, 2010, **651**, 251.
28. E. Achenbach, *J. Fluid Mech.*, 1972, **54**, 565.
29. H. Schlichting, *Boundary Layer Theory*, McGraw-Hill Book Company, 1979.
30. D. W. Moore, *J. Fluid Mech.*, 1965, **23**, 749.
31. H. Jouhara and B. P. Axcell, *Nucl. Eng. Des.*, 2009, **239**, 1885.

Leidenfrost vapour layer moderation of drag crisis and trajectories of superhydrophobic and hydrophilic spheres falling in water

Ivan U. Vakarelski, Derek Y. C. Chan and Sigurdur T. Thoroddsen

Table of content entry:

We demonstrate that a stable Leidenfrost vapour layer sustained on the surface of a steel sphere falling through water can reduce the hydrodynamic drag by up to 75% and stabilize the sphere trajectory.

